



OPEN Vanadium and tantalum doping of tin dioxide: a theoretical study

Petros-Panagis Filippatos^{1,2}✉, Nikolaos Kelaidis³, Maria Vasilopoulou¹ & Alexander ChronEOS^{4,5}✉

The increasing demand of efficient optoelectronic devices such as photovoltaics has created a great research interest in methods to manipulate the electronic and optical properties of all the layers of the device. Tin dioxide (SnO₂), due to its charge transport capability, high stability and easy fabrication is the main electron transport layer in modern photovoltaics which have achieved a record efficiency. While the wide band gap of SnO₂ makes it an effective electron transport layer, its potential for other energy applications such as photocatalysis is limited. To further improve its conductivity and reduce its bandgap, doping or co-doping with various elements has been proposed. In the present density functional theory (DFT) study, we focus on the investigation of vanadium (V) and tantalum (Ta) doped SnO₂ both in the bulk and the surface. Here we focus on interstitial and substitutional doping aiming to leverage these modifications to enhance the density of states for energy application. These changes also have the potential to influence the optical properties of the material, such as absorption, and make SnO₂ more versatile for photovoltaic and photocatalytic applications. The calculations show the formation of gap states near the band edges which are beneficial for the electron transition and in the case of Ta doping the lowest bandgap value is achieved. Interestingly, in the case of Ta interstitial, deep trap states are formed which depending of the application could be advantageous. Regarding the optical properties, we found that V doping significantly increases the refractive index of SnO₂ while the absorption is generally improved in all the cases. Lastly, we investigate the electronic properties of the (110) surface of SnO₂, and we discuss possible other applications due to surface doping. The present work highlights the importance of V and Ta doping for energy applications and sensor applications.

SnO₂ also known as cassiterite and stannic oxide, represents one of the most used wide bandgap semiconductors in energy devices^{1,2}. It is characterized by n-type conductivity, which can be attributed to its intrinsic defects, such as oxygen vacancies³ and tin interstitials⁴. As a compound, SnO₂ exhibits low resistivity⁵ and high-dielectric constant, and has therefore been considered for gate oxides on Si-based electronic devices^{6,7} as well as for electron transport layer in perovskite photovoltaics⁸. Undoped SnO₂ has a wide bandgap value of ~3.6 eV⁹ and its reported resistivity values range from 10⁻² to 10⁻³ Ω cm¹⁰. One of the main quests in photovoltaic technologies is to enhance the conductivity of the electron transport layer without reducing the bandgap¹¹. In essence, the efficiency of the devices is highly connected with the charge recombination and losses due to the limited transport properties of the used layers. Furthermore, the stoichiometric SnO₂ exhibits low intrinsic carrier density and low mobility of its charges due to the oxygen vacancies which act as donors. Doping is examined as a strategy to further reduce the resistance of SnO₂ and to enhance the transition in the visible wavelengths^{12,13}. For photocatalysis, it is important to increase the conductivity of the photocatalyst and decrease the bandgap of the semiconductor. The increase in the carrier concentration makes the intermediate energy gap between valence band and conduction band more active¹⁴.

To further improve the response of gas sensing devices and improve the sensitivity and selectivity, it is common to add porous materials and catalytically active agents^{15,16}. Doping the metal oxide -such as SnO₂- based sensor promotes the physicochemical reactions between the surface and the gas¹⁷. Various reports propose that incorporation of the appropriate dopant is an efficient technique to enhance the sensitivity, selectivity, operating temperature and recovery time of SnO₂ based gas sensor as the dopant modifies the structural, electronic

¹Institute of Nanoscience and Nanotechnology (INN), National Center for Scientific Research Demokritos, Agia Paraskevi, 15310 Athens, Greece. ²Faculty of Engineering, Environment and Computing, Coventry University, Priory Street, Coventry CV1 5FB, UK. ³Theoretical and Physical Chemistry Institute, National Hellenic Research Foundation, Vass. Constantinou 48, 11635 Athens, Greece. ⁴Department of Materials, Imperial College, London SW7 2AZ, UK. ⁵Department of Electrical and Computer Engineering, University of Thessaly, 38221 Volos, Greece. ✉email: filippap@coventry.ac.uk; alexander.chroneos@imperial.ac.uk

and optical properties of the host compound^{18,19}. Transition metal elements such as Zn, Mn, Cr etc. have been proposed by researchers as successful dopants which enhance the response and selectivity of SnO₂^{20–23}. Although various studies^{24–26} have explored the electrical and optical properties of Ta doped SnO₂, the applications of this doping method in gas sensor has not been reported or examined. Interestingly, Liu et al.²⁷ developed a Ta:SnO₂ electron transport layer (ETL) for high efficiency perovskite solar cells. Ben Soltan et al.²⁸ developed V:SnO₂ nanoparticles for photocatalytic applications.

Here we employ hybrid functional DFT to investigate the impact of substitutional and interstitial doped V and Ta doped bulk and (110) surface SnO₂.

Methodology

The Cambridge Serial Total Energy Package (CASTEP)²⁹ was used. To encounter the effect of localized electrons and bandgap underestimation we employed the hybrid functional PBE0 with norm conserving pseudopotentials³⁰. Convergence tests revealed that a cutoff energy was chosen of 800 eV and $2 \times 2 \times 3$ k-points for the sampling of the Brillouin zone were sufficient for the 48 atom supercell ($2 \times 2 \times 2$ unit cells). The supercell was chosen by taking into account that although hybrid functionals can provide more reliable results, they are very computationally expensive. For the optimization of the relaxed structures and the prediction of the ground state of each system, we used the Broyden–Fletcher–Goldfarb–Shanno (BFGS) method which was seen to predict the correct ground state to various different systems³¹. For the interstitial positions we examined all possible configurations in the supercell in conjunction with geometry optimization and retained the lowest energy configuration. Specifically, we placed the interstitial defects in various sites and we used as the final ground state the configuration with the minimum total energy. The surface simulation was based on a slab model with a vacuum of about 12 Å vertical to the (110) direction. Here, the top two layers represent the surface, whereas the bottom two layers are fixed and represent the bulk region. Considering the DOS calculations a k-point mesh of $5 \times 5 \times 5$ was used for bulk and $3 \times 3 \times 1$ set for the surface. We set the convergence criteria at 2.0×10^{-5} eV/atom for the SCF tolerance, 0.05 eV/Å for the force tolerance and 0.001 Å for the max displacement tolerance.

Results and discussion

Bulk SnO₂

Here we considered SnO₂ in the rutile structure (space group number $P4_2/mmm$), with determined unit cell parameters $a = b = 4.737$ Å and $c = 3.186$ Å and our DFT calculated unit cell parameters are $a = b = 4.717$ Å and $c = 3.189$ Å¹⁴. In Fig. 1, we report the minimum energy configurations with relevant nearest neighbour distances and angles of (a) Ta substitutional doped SnO₂ (Ta_{Sn}:SnO₂), (b) Ta interstitial doped SnO₂ (Ta_i:SnO₂), (c) V substitutional doped SnO₂ (V_{Sn}:SnO₂), (d) V interstitial doped SnO₂ (V_i:SnO₂) and (e) the undoped 48-atom

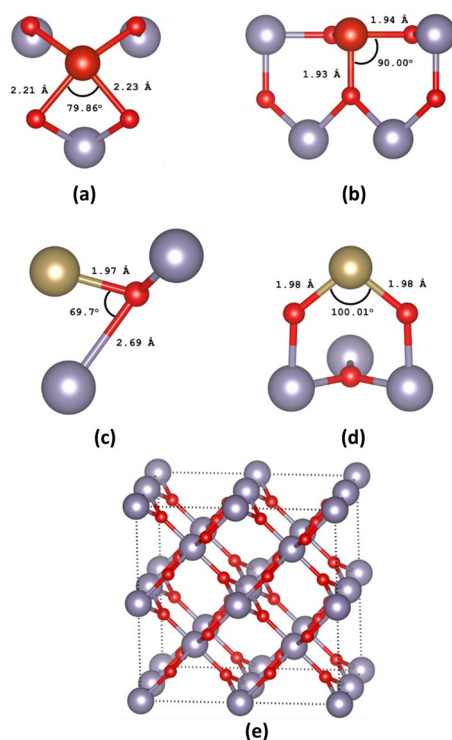


Figure 1. The minimum energy configurations of (a) Ta substitutional doped SnO₂ (Ta_{Sn}:SnO₂), (b) Ta interstitial doped SnO₂ (Ta_i:SnO₂), (c) V substitutional doped SnO₂ (V_{Sn}:SnO₂), (d) V interstitial doped SnO₂ (V_i:SnO₂) and (e) the supercell.

supercell. We have considered all the possible configurations of these defects in the supercell but the subsequent figures report results on the minimum energy configurations only.

In Table 1 we have gathered the lattice parameters for all the doping cases. As it is seen, in all the cases except the vanadium substitutional, the volume of the unit cell increases. Typically, a larger supercell is connected to larger area for the chemical reactions to take place and can lead to improved photocatalytic activity of SnO₂. Our approach agrees well with experimental reports^{23,32}. Specifically, Alvarez-Roca et al.²³ investigated at various vanadium doping concentration the X-ray diffraction and transmittance electron microscope for the determination of the structural changes in SnO₂. Similar to our study, they found that the V atoms can be incorporated inside the structure of SnO₂ and at low concentrations the cell volume is reduced. According to their study, this reduction enhances the specific surface area to volume ration which is highly beneficial for applications of V:SnO₂ in catalysis, sensors and energy applications. Continuing with the recent work of Uwhoreye et al.³², where they investigated the structural, electronic and optical properties of Ta:SnO₂ thin films, they found that at low Ta concentrations, the lattice parameters of SnO₂ are slightly reduced with the volume remaining almost unchanged. At low concentrations the incorporation of Ta atoms takes place in Sn sites and due to the smaller radius of Ta atoms (0.064 nm) compared to Sn atoms (0.065 nm) this leads to relative decrease of the lattice parameters. As they report, at higher concentration this phenomenon is reversed and the volume is increased. We believe that this is happening because at higher concentrations it is more likely for interstitials to form, and as we show, Ta_i:SnO₂ exhibits a higher volume than Ta_{Sn}:SnO₂. While our work predicts similar trends with the above mentioned experimental works, in order to explain completely and with great accuracy the above mentioned experimental results, different doping concentration should be examined, which is beyond of the scope of this paper. Ali and Islam³³ investigated using DFT the effect of Ta doping in SnO₂ and they also predicted that incorporation of Ta in SnO₂ increases the volume of the supercell.

Continuing our work with the electronic investigation of Ta/V doped SnO₂ we report in Fig. 2 the calculated total DOS and the (partial) PDOS for each doping case. As it is shown in Fig. 2e, the hybrid functional DFT calculations using PBE0 result in a bandgap value of 3.35 eV¹³, in excellent agreement with the experimentally determined bandgap²³. Doping with Ta_i or V_i will result in a small increase of the band gap, however Ta and V at substitutional sites reduce the band gap by about 0.5 eV (refer to Table 2). Overall, The decrease of the band gap for the V and Ta doping, is caused by the overlapping of V-3d (Ta-3d) with O-2p. Those overlapping could initiate the formation not only of states near the band edges but also of intermediate bands (deep states). The increase of the bandgap in Ta_i could be attributed to the effect of electron doping which is responsible for shifting the fermi level into the conduction band, this phenomenon is also called Burstein-Moss effect³⁴.

For both V_i:SnO₂ (Fig. 2a) and Ta_i:SnO₂ (Fig. 2c) in gap states form to the conduction band edge and the bandgap calculated to increase to 3.39 eV and 3.48 eV, respectively (Table 2). This formation of energy states in the middle of the bandgap can be advantageous for photocatalytic applications, however it is detrimental for photovoltaics and light emission diodes as they act as traps that reduce the device photocurrent and photogenerated charge carriers. Conversely, for V_{Sn}:SnO₂ (Fig. 2b) and Ta_{Sn}:SnO₂ (Fig. 2d) the band gap is reduced to 2.86 eV and 2.84 eV, respectively (refer to Table 1). This band gap reduction is attractive for photocatalytic applications.

Figure 3 reports the refractive index with respect the phonon energy for all the doping cases considered. For zero frequency the refractive index is predicted to be a 1.40, in excellent agreement with previous theoretical studies but lower as compared to the experimental value (1.70)^{35,36}. From Table 2 and Fig. 3 it is clear that there is an increase for the lower photon energies and a decrease in the upper energies.

Figure 4 reports the reflectivity (i.e. amount of photons that are reflected) and it is predicted that V_i:SnO₂ has the highest reflectivity in the near-infrared region (refer to Table 2). Ta-doped SnO₂ has low reflectivity in the infrared and visible region therefore it can be used as an antireflective coating.

In Fig. 5a,b present the optical conductivity and absorption coefficient for all the doping cases considered here. The optical conductivity is effectively represented by the mobility of excitons (electron–hole pairs) a crucial parameter in the design of optical detectors³⁷. The excitons are generated when photons have higher energy than the optical bandgap and because of the electronic charge neutrality do not contribute to the electrical conductivity³⁸. The absorption of undoped SnO₂ starts at 380 nm in fair agreement with the experimental value (400 nm)³⁹. From Fig. 5b it is observed that that Ta_i and V_i have the highest absorption in the visible region.

Surface SnO₂

The investigation of the most exposed surface, in this case the (110) surface¹³, is of crucial importance for the application of doped SnO₂ to various technologies such as gas sensors⁴⁰ and photocatalytic hydrogen production⁴¹. Specifically for the gas sensors the adsorption and desorption of oxygen and gas molecules occurs on the surfaces of the material while for the hydrogen production the most high-energetic surface will play the

	a(Å)	c(Å)	Vol (Å ³)
SnO ₂	4.71	3.18	70.95
V _{Sn} :SnO ₂	4.69	3.18	69.95
V _i :SnO ₂	4.89	3.21	76.76
Ta _{Sn} :SnO ₂	4.72	3.19	71.07
Ta _i :SnO ₂	4.94	3.20	78.09

Table 1. Lattice parameters of Ta and V doped SnO₂.

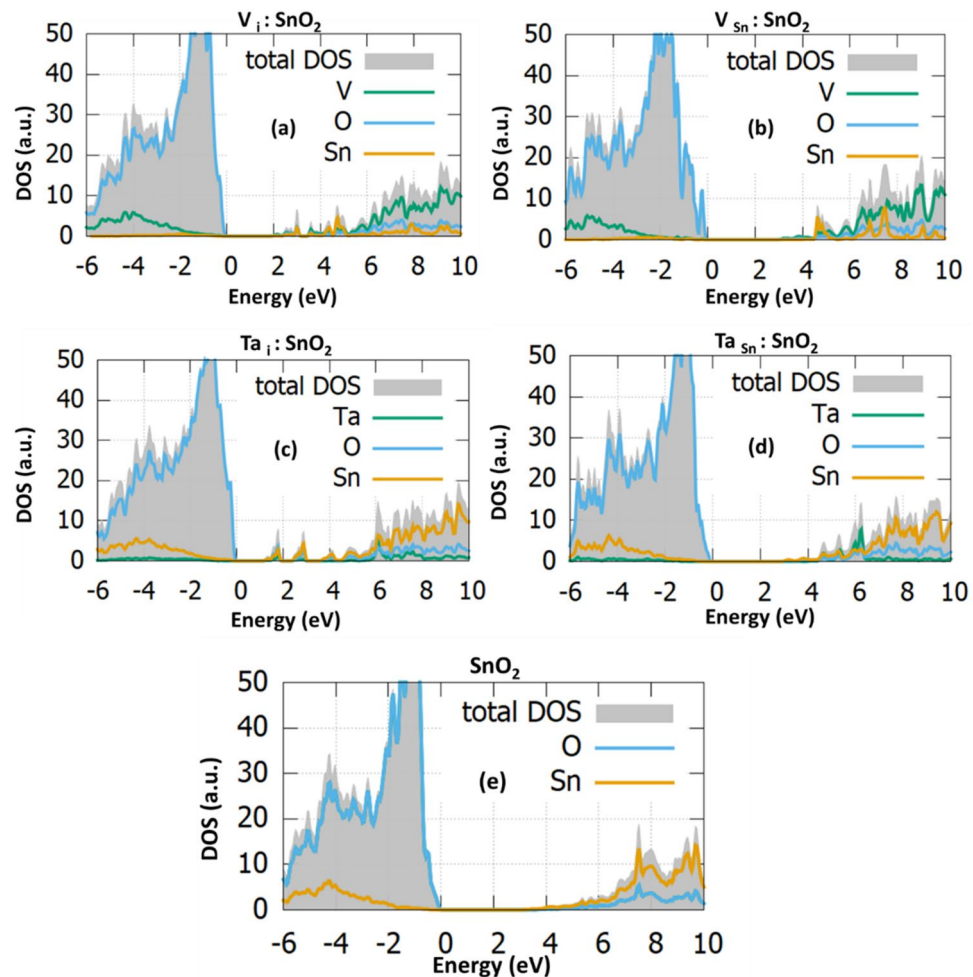


Figure 2. The total DOS and the projected density of states (PDOS) of (a) $V_i:SnO_2$, (b) $V_{Sn}:SnO_2$, (c) $Ta_i:SnO_2$, (d) $Ta_{Sn}:SnO_2$, and (e) undoped SnO_2 .

	Bandgap	Refractive index	Reflectivity
SnO_2	3.35	1.40	0.03
$V_i:SnO_2$	3.39	1.50	0.35
$V_{Sn}:SnO_2$	2.86	2.25	0.15
$Ta_i:SnO_2$	3.48	2.10	0.12
$Ta_{Sn}:SnO_2$	2.84	1.60	0.05

Table 2. The predicted electronic and optical constants.

role of the active site in photocatalytic reactions. As it is seen from the available literature, the studies of the (110) SnO_2 surface are significantly less compared to the studies of the bulk.

In this section, the electronic density of states changes of the undoped and the V, Ta doped SnO_2 were investigated. The (110) surface is cleaved from the bulk SnO_2 and it is represented with a nine-layer slab model, as it is presented in Fig. 6. The (110) surface consists of 16 SnO_2 atoms and 32 O atoms while the size of the vacuum is chosen at 12 Å. For our calculations the bottom 4 layers are kept fixed during the geometry optimization in order to represent the bulk side while the top 5 are free to relax for the energy minimization. Our model has been used to various other studies, such as were the adsorption of hydrogen molecules on Cu-doped SnO_2 surface is chosen⁴². Similarly, the same process was followed in this paper in order to simulate the minimum energy system for the doped surface. Furthermore, to accurately predict the DOS characteristics the hybrid functional PBE0 was used.

The total Density of states of the undoped and the V, Ta-doped SnO_2 surface, as well as the partial density of states of O, Sn, V and Ta atom as are depicted in Fig. 7a–c. From our results in Fig. 7a it can be seen that V doping produces a surface band gap of nearly 2 eV. Compared to the pure SnO_2 (110) facet it can be observed

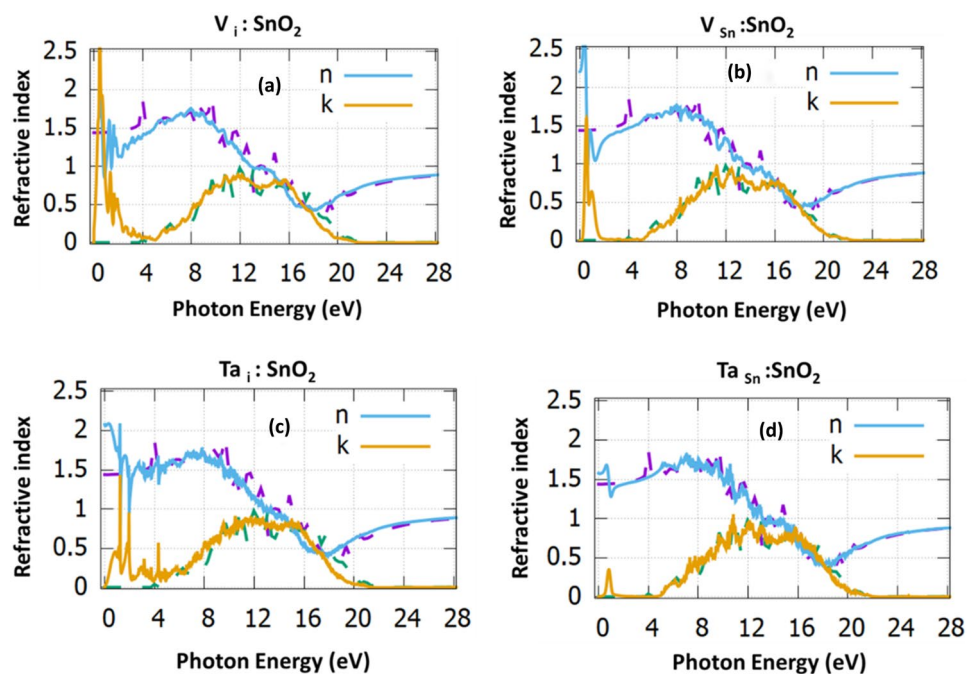


Figure 3. The refractive index for (a) $V_i:SnO_2$, (b) $V_{Sn}:SnO_2$, (c) $Ta_i:SnO_2$ and (d) $Ta_{Sn}:SnO_2$. The dotted purple and dotted green, correspond to the dielectric function of the undoped SnO_2 .

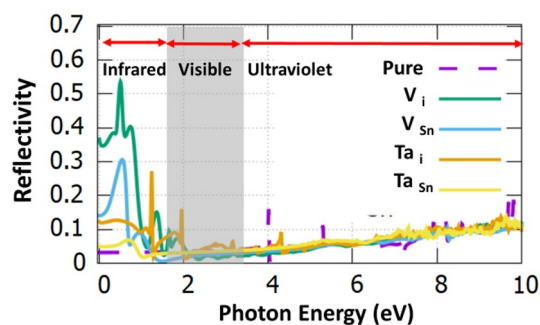


Figure 4. The reflectivity of the doped structures. The dotted purple line corresponds to undoped SnO_2 .

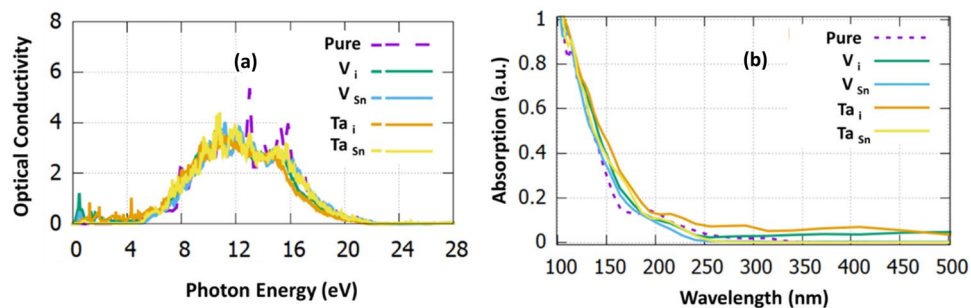


Figure 5. (a) The optical conductivity with respect to the photon energy and (b) the absorption coefficient with respect to the wavelength for the investigated dopants.

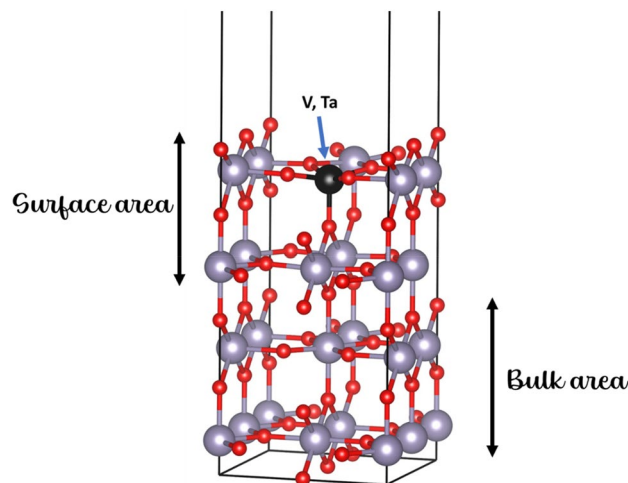


Figure 6. The slab model used for the V, Ta doped SnO₂.

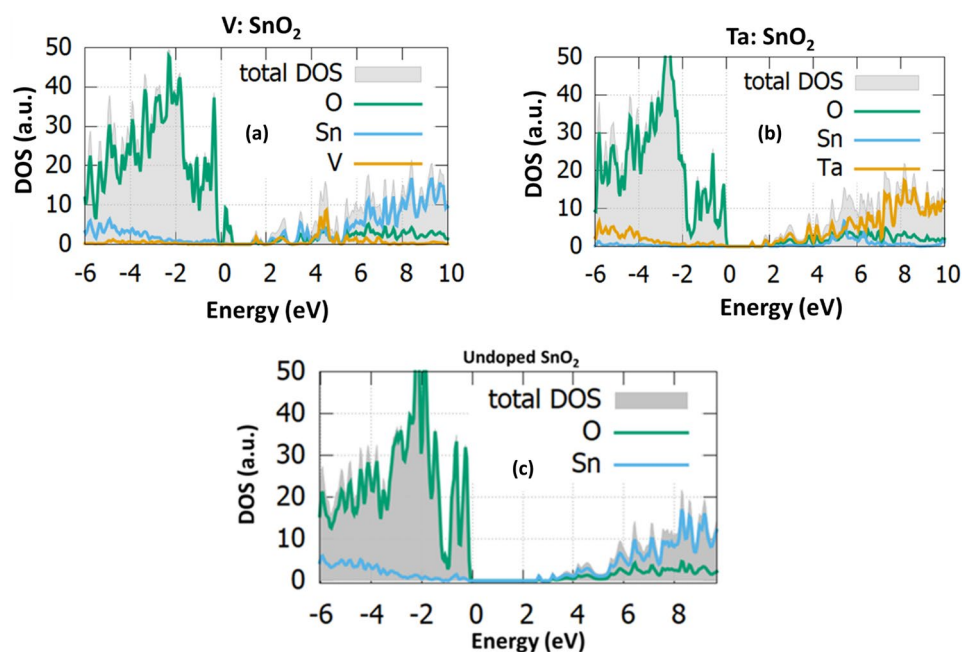


Figure 7. The total density of states (DOS) and the projected density of states (PDOS) of (a) V, (b) Ta and (c) undoped (110) SnO₂ facet.

that the valence band is increased after V doping as some additional states are created at 0.5 eV. Our analysis shows that V doping reduces the bandgap of approximately 0.5 eV. Moreover, additional states are created at the conduction band edge. Continuing with the Ta doping, it can be observed that the bandgap is reduced to a value equal to 1.8 eV while the only energy states that arise are located at 1 eV. Compared to the undoped, Ta doping reduces the bandgap nearly 0.7 eV.

From the surface simulations it can be concluded that gap states that serve as electron traps are formed near the conduction band in all the doping cases. As these trap states are of great importance for the gas sensors and photocatalysis and so further experimental investigation is suggested.

Conclusions

In the present DFT investigation the structural, electronic and optical properties of V and Ta doped SnO₂ were calculated. Our first principles studies investigated the potential of these doping techniques for energy and sensing applications as it involved advanced hybrid calculations both for the bulk and the surface of SnO₂. The DOS calculations revealed that there is a small bandgap increase for Ta_i and V_i doping, whereas for both the Ta and V substitutionals, the bandgap is decreased. Our calculations for the bulk agree well with other experimental reports and explain the trends that could be seen in them. The reduction of the bandgap in the substitutional

cases and the mid-gap states for the interstitial cases can be beneficial for photocatalytic applications while when the band gap is increased especially in the V_i case this can be beneficial for other applications such as electron transport layers. Furthermore, surface calculations indicate that these systems can be applicable for gas sensors as they can provide active sites for the sensing reactions to take place and also the gap states formed can further enhance these reactions. Therefore experimental work is necessary.

Data availability

The datasets used and/or analysed during the current study available from the corresponding author on reasonable request.

Received: 7 August 2023; Accepted: 13 November 2023

Published online: 28 November 2023

References

- Fortunato, E., Ginley, D., Hosono, H. & Paine, D. C. Transparent conducting oxides for photovoltaics. *MRS Bull.* **32**, 242–247 (2007).
- Mallikarjuna, K., Rafiqul Bari, G. A. K. M., Vattikuti, S. V. P. & Kim, H. Synthesis of carbon-doped SnO₂ nanostructures for visible-light-driven photocatalytic hydrogen production from water splitting. *Int. J. Hydrog. Energy* **45**, 32789–32796 (2020).
- Trani, F., Causà, M., Ninno, D., Cantele, G. & Barone, V. Density functional study of oxygen vacancies at the SnO₂ surface and subsurface sites. *Phys. Rev. B* **77**, 245410 (2008).
- Villamagua, L. *et al.* Change in the electrical conductivity of SnO₂ crystal from n-type to p-type conductivity. *Chem. Phys.* **452**, 71–77 (2015).
- Isono, T. *et al.* Highly conductive SnO₂ thin films for flat-panel displays. *J. Soc. Inf. Disp.* **15**, 161 (2007).
- Robertson, J. High dielectric constant gate oxides for metal oxide Si transistors. *Rep. Prog. Phys.* **69**, 327–396 (2006).
- Zunger, A., Kiliç, C. & Wang, L. Defects in photovoltaic materials and the origin of failure to dope them. in *Conference Record of the Twenty-Ninth IEEE Photovoltaic Specialists Conference, 2002* 500–503 (IEEE, 2002). <https://doi.org/10.1109/PVSC.2002.1190611>
- Vasilopoulou, M. *et al.* Charge transport materials for mesoscopic perovskite solar cells. *J. Mater. Chem. C* **10**, 11063–11104 (2022).
- Zhou, W., Liu, Y., Yang, Y. & Wu, P. Band gap engineering of SnO₂ by epitaxial strain: Experimental and theoretical investigations. *J. Phys. Chem. C* **118**, 6448–6453 (2014).
- Batzill, M. & Diebold, U. The surface and materials science of tin oxide. *Prog. Surf. Sci.* **79**, 47–154 (2005).
- Le Corre, V. M. *et al.* Charge transport layers limiting the efficiency of perovskite solar cells: How to optimize conductivity, doping, and thickness. *ACS Appl. Energy Mater.* **2**, 6280–6287 (2019).
- Filippatos, P.-P., Kelaidis, N., Vasilopoulou, M., Davazoglou, D. & Chroneos, A. Defect processes in halogen doped SnO₂. *Appl. Sci.* **11**, 551 (2021).
- Filippatos, P.-P., Kelaidis, N., Vasilopoulou, M., Davazoglou, D. & Chroneos, A. Impact of boron and indium doping on the structural, electronic and optical properties of SnO₂. *Sci. Rep.* **11**, 13031 (2021).
- Zhang, P., Hong, R. Y., Chen, Q. & Feng, W. G. On the electrical conductivity and photocatalytic activity of aluminum-doped zinc oxide. *Powder Technol.* **253**, 360–367 (2014).
- Menil, F., Lucat, C. & Debeda, H. The thick-film route to selective gas sensors. *Sens. Actuators B Chem.* **25**, 415–420 (1995).
- Ivanov, P. *et al.* Development of high sensitivity ethanol gas sensors based on Pt-doped SnO₂ surfaces. *Sens. Actuators B Chem.* **99**, 201–206 (2004).
- Barbosa, M. S. *et al.* Gas sensor properties of Ag- and Pd-decorated SnO micro-disks to NO₂, H₂ and CO: Catalyst enhanced sensor response and selectivity. *Sens. Actuators B Chem.* **239**, 253–261 (2017).
- Lin, Y. *et al.* Synergistically improved formaldehyde gas sensing properties of SnO₂ microspheres by indium and palladium co-doping. *Ceram. Int.* **41**, 7329–7336 (2015).
- Kim, H.-J. & Lee, J.-H. Highly sensitive and selective gas sensors using p-type oxide semiconductors: Overview. *Sens. Actuators B Chem.* **192**, 607–627 (2014).
- Rajeshwaran, P. & Sivarajan, A. Influence of Mn doping on structural, optical and acetone gas sensing properties of SnO₂ nanoparticles by a novel microwave technique. *J. Mater. Sci. Mater. Electron.* **26**, 539–546 (2015).
- Bagwasi, S., Tian, B., Zhang, J. & Nasir, M. Synthesis, characterization and application of bismuth and boron Co-doped TiO₂: A visible light active photocatalyst. *Chem. Eng. J.* **217**, 108–118 (2013).
- Kou, X. *et al.* Synthesis of Co-doped SnO₂ nanofibers and their enhanced gas-sensing properties. *Sens. Actuators B Chem.* **236**, 425–432 (2016).
- Alvarez-Roca, R., Desimone, M., Da Silva, M. G. S., Ponce, M. A. & Longo, E. Vanadium doping effect on multifunctionality of SnO₂ nanoparticles. *J. Mater. Appl.* **9**, 38–45 (2020).
- Slassi, A. Ab initio study on the structural, electronic, optical and electrical properties of Mo-, Nb- and Ta-doped rutile SnO₂. *Opt. Quantum Electron.* **48**, 160 (2016).
- Maleki, M. Ab initio calculations of the effect of N, Nb, and Ta doping on the electronic structure and optical properties of SnO₂. *J. Comput. Electron.* **19**, 47–54 (2020).
- Williamson, B. A. D. *et al.* Resonant Ta doping for enhanced mobility in transparent conducting SnO₂. *Chem. Mater.* **32**, 1964–1973 (2020).
- Liu, Q. *et al.* Effect of tantalum doping on SnO₂ electron transport layer via low temperature process for perovskite solar cells. *Appl. Phys. Lett.* **115**, 143903 (2019).
- Soltan, W. B., Lassoued, M. S., Ammar, S. & Toupance, T. Vanadium doped SnO₂ nanoparticles for photocatalytic degradation of methylene blue. *J. Mater. Sci. Mater. Electron.* **28**, 15826–15834 (2017).
- Segall, M. D. *et al.* First-principles simulation: Ideas, illustrations and the CASTEP code. *J. Phys. Condens. Matter* **14**, 2717–2744 (2002).
- Paier, J. *et al.* Screened hybrid density functionals applied to solids. *J. Chem. Phys.* **124**, 154709 (2006).
- Qureshi, M. W. *et al.* Verification of stability and unraveling the electronic and physical properties of bulk and (001)-surfaces of newly synthesized Ti₂ZnX (X = C, N) MAX phases. *Surf. Interfaces* **31**, 102032 (2022).
- Uwihoreye, V. *et al.* Transparent conductive SnO₂ thin films via resonant Ta doping. *Sci. China Mater.* **66**, 264–271 (2023).
- Ali, M. A. & Islam, A. K. M. A. Sn_{1-x}Bi_xO₂ and Sn_{1-x}Ta_xO₂ (0 ≤ x ≤ 0.75): A first-principles study. *Phys. B Condens. Matter* **407**, 1020–1026 (2012).
- Turgut, G. Effect of Ta doping on the characteristic features of spray-coated SnO₂. *Thin Solid Films* **594**, 56–66 (2015).
- Afiy, H. H., Momtaz, R. S., Badawy, W. A. & Nasser, S. A. Some physical properties of fluorine-doped SnO₂ films prepared by spray pyrolysis. *J. Mater. Sci. Mater. Electron.* **2**, 40–45 (1991).

36. Khan, A. F., Mehmood, M., Aslam, M. & Ashraf, M. Characteristics of electron beam evaporated nanocrystalline SnO₂ thin films annealed in air. *Appl. Surf. Sci.* **256**, 2252–2258 (2010).
37. Akinlami, J. O. & Olateju, I. O. Reflection coefficient and optical conductivity of gallium nitride GaN. *Semicond. Phys. Quantum Electron. Optoelectron.* **15**, 281–284 (2012).
38. Dash, L. K., Vast, N., Baranek, P., Cheynet, M.-C. & Reining, L. Electronic structure and electron energy-loss spectroscopy of ZrO₂ zirconia. *Phys. Rev. B* **70**, 245116 (2004).
39. Doyan, A., Susilawati, S. & Imawanti, Y. D. Synthesis and characterization of SnO₂ thin layer with a doping aluminum is deposited on quartz substrates. *AIP Conf. Proc.* **1801**, 020005. <https://doi.org/10.1063/1.4973083> (2017).
40. Filippatos, P.-P. *et al.* Optimization of the hydrogen response characteristics of halogen-doped SnO₂. *Sci. Rep.* **13**, 2524 (2023).
41. Talebian, N. & Jafarinezhad, F. Morphology-controlled synthesis of SnO₂ nanostructures using hydrothermal method and their photocatalytic applications. *Ceram. Int.* **39**, 8311–8317 (2013).
42. Wang, F. *et al.* Adsorption mechanism of Cu-doped SnO₂ (110) surface toward H₂ dissolved in power transformer. *J. Nanomater.* **2016**, 1–9 (2016).

Acknowledgements

The open access fee was paid from the Imperial College London Open Access Fund.

Author contributions

P.P.F. performed the calculations, P.P.F. and A.C. wrote the main manuscript. All authors contributed and reviewed the manuscript.

Competing interests

The authors declare no competing interests.

Additional information

Correspondence and requests for materials should be addressed to P.-P.F. or A.C.

Reprints and permissions information is available at www.nature.com/reprints.

Publisher's note Springer Nature remains neutral with regard to jurisdictional claims in published maps and institutional affiliations.



Open Access This article is licensed under a Creative Commons Attribution 4.0 International License, which permits use, sharing, adaptation, distribution and reproduction in any medium or format, as long as you give appropriate credit to the original author(s) and the source, provide a link to the Creative Commons licence, and indicate if changes were made. The images or other third party material in this article are included in the article's Creative Commons licence, unless indicated otherwise in a credit line to the material. If material is not included in the article's Creative Commons licence and your intended use is not permitted by statutory regulation or exceeds the permitted use, you will need to obtain permission directly from the copyright holder. To view a copy of this licence, visit <http://creativecommons.org/licenses/by/4.0/>.

© The Author(s) 2023